American Mineralogist, Volume 75, pages 992–1008, 1990

The amblygonite-montebrasite series: Characterization by single-crystal structure refinement, infrared spectroscopy, and multinuclear MAS-NMR spectroscopy

LEE A. GROAT,* MATI RAUDSEPP, FRANK C. HAWTHORNE
Department of Geological Sciences, University of Manitoba, Winnipeg, Manitoba R3T 2N2, Canada
T. SCOTT ERCIT
National Museum of Natural Sciences, Ottawa, Ontario K1P 6P4, Canada
BARBARA L. SHERRIFF**
Department of Geology, McMaster University, Hamilton, Ontario L8S 4M1, Canada
J. STEPHEN HARTMAN
Department of Chemistry, Brock University, St. Catharines, Ontario L2S 3A1, Canada

ABSTRACT

The F ⇌ OH substitution in the amblygonite ($LiAlPO_4F$)-montebrasite ($LiAlPO_4OH$) series has been studied by crystal structure refinement, electron microprobe analysis, infrared spectroscopy, and multinuclear MAS-NMR spectroscopy. The structures of seven compositions fairly equally spaced across the compositional range were refined to R indices of 2–3% using ~1000 reflections/crystal, measured on an automated four-circle diffractometer with Mo$K\alpha$ X-radiation. The ⟨Al-O,OH,F⟩ distances decrease linearly with F ⇌ OH substitution across the series. The Li is positionally disordered into two sites within a six-coordinated cavity. This splitting is small (~0.20 Å) at the montebrasite end of the series, increasing linearly to (~0.40 Å) at the halfway point of the series, and then remaining constant to the amblygonite end. The cell volume shows nonlinear variation with composition, and this quantitatively accounts for the nonlinear variation in the mean refractive index.

Montebrasite samples show a fairly sharp peak at 3390 cm^{-1} in the OH-stretching region of the infrared spectrum, indicative of a fairly strong H bond. With increasing F substitution, the peak becomes weaker, and shifts to lower energies as a result of replacement of F by OH. There is one broad ^{31}P MAS-NMR peak at −15.75 ppm; it shows no change with composition, in line with the unchanging local environment of P across the series. The ^{7}Li spectra have a single broad peak; as the signals are narrower at lower field, the broadening is not due to quadrupolar effects but must reflect the range of environments around the split Li position. Although there are two Al sites in members of the amblygonite-montebrasite series, the ^{27}Al spectra show only one (rather broad) peak, reflecting the similarity of the two Al sites. As F/(F + OH) increases, the ^{27}Al peak shifts to lower field, and the peak width decreases slightly, probably as a result of a decrease in dipolar coupling between the proton and the Al with decreasing OH content.

The consistency of the structural and chemical results indicates that electron microprobe analyses give reliable results for F. Study by electron microprobe showed intergrowth and alteration of members of the amblygonite-montebrasite series. Nearly all the samples examined showed apatite inclusions or veinlets, and amblygonite often has pervasive veining by lacroixite ($NaAlPO_4F$). Lack of Ca and Na in members of the amblygonite-montebrasite series associated with these intergrowths suggests that the latter do not incorporate Na or Ca into their structure; previous analyses with Ca or Na were probably carried out on material with incipient apatite or lacroixite veining.

INTRODUCTION

The amblygonite-montebrasite series shows complete solid solution with ideal composition $LiAlPO_4(F,OH)$; natural members of the series more F-rich than those with F/(F + OH) = 0.65 are uncommon. As outlined by

* Present address: Department of Geological Sciences, University of British Columbia, Vancouver, British Columbia V6T 2B4, Canada.
** Present address: Department of Geological Sciences, University of Manitoba, Winnipeg, Manitoba R3T 2N2, Canada.

0003–004X/90/0910–0992$02.00

Phillips and Griffen (1981) and Greiner and Bloss (1987), these minerals are triclinic, with amblygonite being optically (−) and montebrasite being optically (+); the compositional boundary between the two is at F/(F + OH) = 0.30. Members of the amblygonite-montebrasite series are common constituents of F- and Li-rich granitic pegmatites. They have been examined by many workers, particularly with regard to the development of a rapid physical method for the determination of the F/(F + OH) ratio or the F content (Moss et al., 1969; Dubois et al., 1972; Černá et al., 1973; Fransolet and Tarte, 1977; Kallio, 1978; Greiner and Bloss, 1987). Inherent in this work is the idea that the OH ⇌ F substitution in minerals is straightforward and uncomplicated, with none of the problems commonly associated with cation ordering, the formation of domains, etc. Some work suggests that this may not be the case. For example, F-rich topaz is orthorhombic, and it has long been assumed that OH-rich topaz has the same symmetry. However, careful structural work (Parise et al., 1980) has shown that OH-rich topaz is triclinic, with an ordered arrangement of H atoms incompatible with orthorhombic symmetry. Thus the topaz solid-solution series with F ⇌ OH is not a simple one, and the F ⇌ OH substitution seems to be more complicated than has generally been assumed. We decided to examine the amblygonite-montebrasite series to see if any interesting complications would come to light.

Natural members of the series generally show little cation substitution. Despite the fact that tavorite ($LiFe^{3+}PO_4F$) is isostructural with amblygonite, Al ⇌ Fe substitution is rare to nonexistent. Some analyses do show minor Na_2O or CaO, but this may be due to contamination, as very careful work (A. M. Fransolet, 1986 personal communication) shows such substitutions to be negligible in this series.

The structures of amblygonite and montebrasite were solved by Simonov and Belov (1958) and Baur (1959a, 1959b). There is an interesting difference between the two structure results. Simonov and Belov (1958) noted that the Li position in amblygonite seemed to be split into two half-atoms, whereas Baur (1959b) did not find such splitting in the structure of montebrasite. These early results suggest that these minerals do not have a simple solid-solution relationship, giving further encouragement for a more detailed study. Preliminary reports of this current work are given by Groat et al. (1987a, 1987b).

Experimental

The material used in this work was obtained from Dr. Petr Černý, University of Manitoba. Most of the samples were used by Černá et al. (1973), and their sample numbers are retained in this work; these were supplemented by an additional F-rich sample (M6116) from the University of Manitoba departmental collection.

Electron microprobe analyses

Electron microprobe analyses were carried out at the National Museum of Natural Sciences, Ottawa, using a JEOL 733 microprobe with Tracor Northern 5500 and 5600 automation. The operating potential was 15 kV and a beam current of 20 nA was used. The beam diameter was set at 30 μm as a safeguard against specimen damage during electron bombardment. Data for standards were measured for 25 s or 0.25% precision per element, whichever was attained first; data for the samples were measured for 25 s or to 0.5% precision, whichever was attained first. Standards were apatite (Ca$K\alpha$, P$K\alpha$), topaz (Al$K\alpha$, F$K\alpha$), albite (Na$K\alpha$), sanidine (K$K\alpha$), and almandine (Fe$K\alpha$). Of the above elements, Fe and Ca were not detected ($I < 4\sigma[I]$); furthermore, no other elements with $Z > 11$ were observed in energy-dispersive spectra measured on some of the grains. Operating conditions were highly stable; consequently, calibrations on the standards were carried out only at the beginning of each experiment. All measurements were carried out with wavelength spectrometers. Because the F$K\alpha$ peaks for topaz and amblygonite are very similar in shape, peak heights were found to be a good measure of the true peak intensity; consequently, peak heights were used in the ZAF calculations. Data reduction was carried out with a conventional ZAF routine in the Tracor Northern Task series of programs. Where possible, two analyses were measured on fresh regions of each sample: center and edge analyses for large grains, and on separate grains for small samples. In some cases, it was impossible to avoid altered regions; pervasive lacroixite alteration was particularly extensive, and probably accounts for higher Na in the analysis of samples AF-65(1), (2).

Formulae were calculated on a basis of 5(O + OH + F); Li_2O and H_2O were calculated according to stoichiometry: Li = 1 − (Na + K), OH = 1 − F. The final analyses are given in Table 1. Table 2 is a list of all phases associated with each amblygonite-montebrasite sample.

Single-crystal photography

Single-crystal X-ray precession photographs of samples AF-65, AF-46, and AF-47 indicated triclinic symmetry with cell dimensions and extinction conditions (none) as found in previous studies. However, rather than use the primitive cell of previous work, we used an alternate *C*-centered cell. This *C*-centered cell is pseudomonoclinic and emphasizes the structural relationships with the kieserite and titanite group minerals (Baur, 1959a; Hawthorne et al., 1987).

X-ray intensity data

Each crystal was mounted on a Nicolet $R3m$ automated four-circle diffractometer. A random-orientation rotation photograph was used to determine starting parameters from which 25 intense reflections were automatically aligned. Least-squares refinement of the setting angles of these reflections gave the cell dimensions in Table 3, together with an orientation matrix relating the crystal axes to the diffractometer axes.

Intensity data were measured in the θ:2θ scan mode according to the experimental procedure of Hawthorne

TABLE 1. Amblygonite-montebrasite analyses

	1	2	3	4	5	6	7	8	9	10	11	12	13	14	15	16
Li_2O*	10.09	10.09	10.09	10.15	10.13	10.12	10.07	10.10	10.07	10.13	10.18	10.13	10.11	10.12	10.08	10.10
Na_2O	—	—	—	—	—	—	—	—	—	—	—	—	—	—	0.07	0.09
K_2O	—	—	—	—	—	—	—	—	—	—	—	—	—	0.04	—	—
Al_2O_3	33.76	33.98	33.86	34.09	33.77	33.81	33.92	33.93	33.89	33.86	34.48	34.02	34.02	34.13	33.77	33.96
P_2O_5	48.52	48.30	48.40	48.65	48.76	48.70	48.22	48.44	48.20	48.68	48.60	48.61	48.43	48.47	48.60	48.61
H_2O*	3.45	3.29	4.52	3.87	4.31	4.23	3.75	3.65	4.13	4.38	3.23	3.09	3.94	4.03	2.65	2.87
F	5.56	5.90	3.30	4.74	3.79	3.96	4.89	5.14	4.10	3.64	6.14	6.37	4.55	4.39	7.26	6.83
O = F	−2.34	−2.48	−1.39	−2.00	−1.60	−1.67	−2.06	−2.16	−1.73	−1.53	−2.59	−2.68	−1.92	−1.85	−3.06	−2.88
Total	99.04	99.08	98.78	99.50	99.16	99.15	98.79	99.10	98.66	99.16	100.04	99.54	99.13	99.33	99.37	99.58
Formula contents per 5 (O, OH, F)																
Li	1.000	1.000	1.000	1.000	1.000	1.000	1.000	1.000	1.000	1.000	1.000	1.000	1.000	0.999	0.997	0.996
Na	—	—	—	—	—	—	—	—	—	—	—	—	—	—	0.003	0.004
K	—	—	—	—	—	—	—	—	—	—	—	—	—	0.001	—	—
Al	0.980	0.987	0.984	0.985	0.977	0.979	0.987	0.984	0.987	0.980	0.992	0.984	0.986	0.988	0.979	0.983
P	1.012	1.008	1.010	1.009	1.014	1.013	1.008	1.009	1.008	1.012	1.005	1.010	1.008	1.007	1.012	1.010
	2.992	2.995	2.993	2.994	2.991	2.992	2.995	2.994	2.995	2.992	2.997	2.994	2.994	2.995	2.991	2.993
OH	0.567	0.540	0.743	0.633	0.706	0.692	0.618	0.600	0.680	0.717	0.526	0.506	0.646	0.659	0.435	0.470
F	0.433	0.460	0.257	0.367	0.294	0.308	0.382	0.400	0.320	0.283	0.474	0.494	0.354	0.341	0.565	0.530
O	4	4	4	4	4	4	4	4	4	4	4	4	4	4	4	4

	17	18	19	20	21	22	23	24	25	26	27	28	29	30	31
Li_2O*	10.15	10.16	10.11	10.06	10.14	10.24	10.21	10.13	10.12	10.22	10.04	9.92	9.97	10.12	9.98
Na_2O	—	—	—	—	—	—	—	—	—	—	0.22	0.20	0.19	—	0.30
K_2O	0.04	—	—	—	0.04	0.04	—	—	—	0.04	—	—	—	—	0.04
Al_2O_3	34.14	34.23	34.01	34.08	33.95	34.29	34.35	33.93	34.24	34.31	33.97	33.56	33.87	33.90	34.13
P_2O_5	48.71	48.63	48.41	47.96	48.82	49.28	48.89	48.64	48.29	49.10	48.68	48.11	48.18	48.44	48.46
H_2O*	5.58	5.74	1.92	1.88	3.06	2.95	6.15	6.11	3.37	3.54	0.73	0.50	2.71	0.00	1.41
F	1.15	0.82	8.80	8.82	6.46	6.81	—	—	5.76	5.55	11.36	11.71	7.09	13.06	9.92
O = F	−0.48	−0.35	−3.71	−3.71	−2.72	−2.87	0.00	0.00	−2.43	−2.34	−4.78	−4.93	−2.99	−5.50	−4.18
Total	99.29	99.23	99.54	99.09	99.75	100.74	99.60	98.81	99.35	100.42	100.22	99.07	99.02	100.02	100.06
Formula contents per 5 (O, OH, F)															
Li	0.999	1.000	1.000	1.000	0.999	0.999	1.000	1.000	1.000	0.999	0.990	0.990	0.991	1.000	0.985
Na	—	—	—	—	—	—	—	—	—	—	0.010	0.010	0.009	—	0.014
K	0.001	—	—	—	0.001	0.001	—	—	—	0.001	—	—	—	—	0.001
Al	0.985	0.987	0.986	0.993	0.980	0.980	0.986	0.982	0.992	0.983	0.982	0.982	0.987	0.982	0.988
P	1.009	1.008	1.008	1.004	1.012	1.012	1.008	1.011	1.005	1.010	1.011	1.011	1.008	1.008	1.007
	2.994	2.995	2.995	2.998	2.992	2.992	2.994	2.993	2.997	2.993	2.993	2.992	2.995	2.990	2.995
OH	0.911	0.937	0.315	0.310	0.500	0.478	1.000	1.000	0.552	0.573	0.119	0.081	0.446	0.000	0.230
F	0.089	0.063	0.685	0.690	0.500	0.522	—	—	0.448	0.427	0.881	0.919	0.554	1.015	0.770
O	4	4	4	4	4	4	4	4	4	4	4	4	4	3.985	4

Note:—not detected. Columns are as follows: 1. A-1 (grain #1, center), 2. A-1 (grain #1, edge), 3. A-1 (grain #2, center), 4. A-1 (grain #2, edge), 5. A-2 (center), 6. A-2 (edge), 7. A-4/5 (center), 8. A-4/5 (edge), 9. A-5dg (grain #1), 10. A-5dg (grain #2), 11. A-29 (center), 12. A-29 (edge), 13. A-60dg (center), 14. A-60dg (edge), 15. AF-1 (center), 16. AF-1 (edge), 17. AF-43 (center), 18. AF-43 (edge), 19. AF-45/46(1) (center), 20. AF-45/46(1) (edge), 21. AF-45/46(2) (center), 22. AF-45/46(2) (edge), 23. AF-47 (center), 24. AF-47 (edge), 25. AF-50 (center), 26. AF-50 (edge), 27. AF-65(1) (center), 28. AF-65(1) (edge), 29. AF-65(2) (center), 30. M6116 (center), 31. M6117 (center).

* Calculated.

Table 2. Mineral phases associated with amblygonite-montebrasite samples used in microprobe study

A-1	Apatite veinlets, very minor wodginite inclusions
A-2	Minor apatite veinlets
A-4/5	Apatite inclusion
A-5dg	(No associates)
A-29	Apatite inclusions, crandallite veinlets, wodginite inclusions
A-60dg	Minor patches of apatite
AF-1	Apatite, lacroixite veinlets, lithiophilite, unknown Sr-Al-Ca phosphate inclusions
AF-43	Apatite veinlets, uranian microlite inclusions
AF-45/46(1)	Unknown Na-Ca-Al phosphate inclusion, unknown aluminosilicate incluson (topaz?)
AF-45/46(2)	Minor apatite veinlets
AF-47	(No associates)
AF-50	Patches and veinlets of crandallite and an unknown Na-Ca-Al phosphate
AF-65(1)	Abundant lacroixite veinlets, one apatite veinlet
AF-65(2)	Abundant lacroixite veinlets, minor apatite veinlets
M6116	Abundant lacroixite veinlets, minor stibiotantalite and apatite inclusions
M6117	Abundant lacroixite veinlets, one apatite veinlet

and Groat (1985); numbers of reflections are given in Table 3, together with other information pertinent to data collection, reduction, and structure refinement. Ten strong reflections uniformly distributed with regard to 2θ were measured at 10° intervals of ψ (the azimuthal angle, corresponding to rotation of the crystal about its diffraction vector) from 0–350°. These data were used to calculate an ellipsoidal shape for the crystal, which was then used in the empirical absorption correction. The data were also corrected for Lorentz, polarization, and background effects and reduced to structure factors; reflections with $I > 2.5\sigma I$ were considered as observed. All routines used in this work were from the SHELXTL system of programs (Sheldrick, 1981).

Infrared spectroscopy

Powdered samples were prepared by grinding by hand about 10 mg of amblygonite-montebrasite with ethanol in an alumina mortar until the grain size was generally less than 2 μm. After drying to cause evaporation of the ethanol, 0.5 mg of sample was mixed with 200 mg of KBr, either grinding by hand in an alumina mortar or in a dentist's amalgamator (Wig-L-Bug). The resulting mixture was dried under vacuum at 125 °C for 20 h, and was then pressed in an evacuated die into a 13-mm pellet.

High-resolution infrared spectra were recorded on a Nicolet Fourier-transform interferometric infrared spectrophotometer, Model MX-1, equipped with a Nicolet 1280 computer for signal processing. The sample chamber was purged with dry N_2 before and after spectrum measurement. Frequency measurements were calibrated internally against a He-Ne laser, and are accurate to 0.01 cm^{-1} according to the manufacturer.

Magic-angle-spinning nuclear-magnetic-resonance spectroscopy

MAS-NMR spectra were obtained on powdered samples using a magic-angle-spinning probe (Fyfe et al., 1982) and Delrin rotors on Bruker WH-400, AC-200, and CXP-200 multinuclear Fourier-transform NMR spectrometers equipped with 9.4, 4.7, and 4.7 T superconducting magnets, respectively. The samples were spun at approximately 3500 Hz at an angle of 54.7° to the magnetic field.

The ^{27}Al MAS-NMR spectra were recorded at 104.23 MHz on the WH-400 spectrometer with 30° pulses, a spectral width of 62500 Hz and a relaxation delay of 0.3 s between pulses. Chemical shifts are reported in ppm with reference to saturated aqueous $[Al(H_2O)_6]^{3+}(ClO_4)_3^-$. The broad ^{27}Al resonances are accurate to within ±0.5 ppm.

Table 3. Data measurement and refinement information: Amblygonite-montebrasite samples

	AF-47	AF-43	A-2	A-1	AF-46	M6116	AF-65
a(Å)	6.713(1)	6.713(1)	6.6984(9)	6.6837(8)	6.6782(8)	6.644(2)	6.6452(9)
b(Å)	7.708(1)	7.711(1)	7.710(1)	7.7080(9)	7.7159(9)	7.744(2)	7.733(1)
c(Å)	7.0194(7)	7.0102(7)	6.983(1)	6.9671(6)	6.949(1)	6.910(1)	6.9193(6)
α(°)	91.31(1)	91.22(1)	91.06(1)	90.94(1)	90.82(1)	90.35(2)	90.35(1)
β(°)	117.93(1)	117.91(1)	117.81(1)	117.75(1)	117.66(1)	117.33(2)	117.44(1)
γ(°)	91.77(1)	91.67(1)	91.49(1)	91.36(1)	91.22(1)	91.01(2)	91.20(1)
V(Å^3)	320.49(8)	320.25(8)	318.70(8)	317.40(6)	316.94(7)	315.8(2)	315.50(7)
Space group	$C\bar{1}$	$C\bar{1}$	$C\bar{1}$	$C\bar{1}$	$C\bar{1}$	$C\bar{1}$	$C\bar{1}$
Z	4	4	4	4	4	4	4
F/F + OH*	0.04	0.08	0.30	0.45	0.59	0.86	0.90(2)
Crystal size (mm)	0.21 × 0.20 ×0.14	0.22 × 0.20 ×0.14	0.20 × 0.20 ×0.12	0.24 × 0.24 ×0.10	0.22 × 0.20 ×0.18	0.18 × 0.26 ×0.14	0.28 × 0.22 ×0.32
Radiation	Mo$K\alpha$	Mo$K\alpha$	Mo$K\alpha$	Mo$K\alpha$	Mo$K\alpha$	Mo$K\alpha$	Mo$K\alpha$
Monochromator	Graphite	Graphite	Graphite	Graphite	Graphite	Graphite	Graphite
R (azimuthal) %	1.2	1.0	0.9	1.0	1.3	0.9	1.0
Total no. $\|F\|$	1013	1014	994	994	993	922	988
No. of $\|F\|$obs	908	908	903	891	895	907	880
R (isotropic)	3.1	4.1	4.1	3.2	5.2	4.0	4.8
R (observed) %	2.2	2.8	2.1	2.2	2.1	2.9	2.4
wR (observed) %	2.5	3.3	2.4	2.6	2.5	3.8	2.7

$R = \Sigma(|F| - |F|)/\Sigma|F|$

$wR = [\Sigma w(|F| - |F|)^2/\Sigma wF^2]^{0.5}$, $w = 1$

* Average of electron microprobe results, this study.

The ^{19}F MAS-NMR spectra were recorded at a frequency of 188.15 MHz on the AC-200 spectrometer with 8192 data points, using a spectral width of 70000 Hz, 20° pulses, and a delay of 5 s between pulses. Chemical shifts are reported in ppm to a low field of $CFCl_3$ with an accuracy of ±0.5 ppm and were determined with reference to a secondary standard of C_6F_6 (−163.1 ppm).

The ^{7}Li MAS-NMR spectra were recorded with 8192 data points and a spectral width of 100 000 Hz at 77.7 MHz on the CXP-200 spectrometer with a relaxation delay of 0.1 s and also on the WH-400 spectrometer at 155.5 MHz with a relaxation delay of 5 s. The ^{6}Li spectra were obtained at a frequency of 44.2 MHz on a Bruker MSL-300 multinuclear spectrometer equipped with a high-speed Doty MAS probe using rotors with a diameter of 5 mm, with 8192 data points, a spectral width of 10000 Hz, and a delay of 1 s between pulses. Chemical shifts are reported with reference to a 70% aqueous solution of LiBr and have an estimated error of ±0.1 ppm.

The ^{31}P MAS-NMR spectra were recorded at 80.96 MHz on the CXP-200 spectrometer with a delay of 5 s between pulses and a spectral width of 80000 Hz. Chemical shifts are reported with reference to H_3PO_4 but were recorded with reference to the two peaks of liquid $MeP(C_6H_5)_3Br$ at 18.4 and 15.3 ppm, with an estimated error of ±0.1 ppm.

Structure refinement

Scattering curves for neutral atoms together with anomalous dispersion coefficients were taken from the *International Tables for X-ray Crystallography,* Vol. IV (1974). *R* indices are of the form given in Table 2 and are expressed as percentages.

Structure refinement was initiated using the atomic positions for montebrasite (Baur, 1959b), modified for the change in unit cell orientation. Refinements converged rapidly to *R* indices of 3–5% for an isotropic displacement model, with the exception of sample AF-1, which will be discussed later. In all refinements, the isotropic displacement factors for Li showed a general increase with increasing F across the series. Conversion to anisotropic displacement factors and full matrix refinement of all variables led to convergence at *R* indices of 2–3%. The anomalous 'thermal' behavior of Li was even more noticeable with anisotropic displacement factors, the displacements being sufficient to suggest (but not confirm) that Li is disordered between two discrete positions. Consequently a split-atom model was used for Li, with two half-occupied Li positions, each constrained to have identical isotropic displacement factors. This model produced no significant difference in the *R* indices, but the magnitudes of the individual isotropic displacement factors for the half-occupied positions were a little more reasonable. Final parameters are given in Table 4, and selected interatomic distances are listed in Table 5.

For the refinement of sample AF-1, final convergence occurred for an *R* index of 8.8%. Inspection of the reflection profiles showed small subsidiary humps on the high 2θ side of major reflections. We selected another crystal, measured intensity data as detailed above, and the refinement converged to an *R* index of 5.3%, again significantly higher than that attained for all the other compositions; repeating this on a third crystal gave an *R* index of 4.5%. We also remounted our first crystal and collected a second set of intensity data; this converged to an *R* index of 7.7%. Details of all refinements are given in Tables 6 and 7.[1] These results suggested some problem with the material, and we examined six more crystals by mounting them on the diffractometer and measuring their cell dimensions. These are given in Table 8; note that the total spread in the cell volume is from 316.29–317.46 Å^3 in this one sample. Observed and calculated structure factors (Table 9) for all refinements are deposited, together with Tables 6, 7, and 8. Bond-valence tables for the near end-member compositions are given in Table 10.

Discussion

Structure

The structure is as found in previous studies. Corner-sharing [Alϕ_5] chains (ϕ = unspecified ligand) extend parallel to the **c**-axis and are further linked along their length by PO_4 tetrahedra to form type I [Al$(PO_4)\phi_3$] chains (Moore, 1970). The tetrahedral vertices not linked to the central octahedral chain cross-link to adjacent chains to form a mixed tetrahedral-octahedral framework. The anion that bridges along the length of the [Alϕ_5] octahedral chain is the OH or F anion, and the Li atom occupies a cavity surrounded by six anions in a distorted octahedral arrangement. The structure of amblygonite is graphically identical to the structures of kieserite ($MgSO_4 \cdot H_2O$) and titanite ($CaTiSiO_4 \cdot O$) (Baur, 1959a; Hawthorne et al., 1987). This relationship is much more apparent with the *C*-centered orientation for amblygonite used here (Fig. 1), as compared with the more conventional primitive orientation used previously. The Na analogue of amblygonite is lacroixite, $NaAl(PO_4)F$, the structure of which was described by Pajunen and Lahti (1985). Lacroixite is isostructural with titanite, and hence we are forced to conclude that amblygonite is triclinic (rather than monoclinic) because of the fact that it has Li rather than Na at the interchain sites.

Chemistry

Wet chemical analyses of members of the amblygonite-montebrasite series usually show minor amounts of components in addition to the nominal ones; most common in this regard are Na and Ca. In this work, Ca was not detected, and considering the frequency of apatite as an associate of amblygonite, traces of Ca in past amblygonite analyses done by bulk methods are probably due to ap-

[1] Copies of Tables 6, 7, 8, and 9 may be ordered as Document AM-90-440 from the Business Office, Mineralogical Society of America. 1130 Seventeenth Street NW, Suite 330, Washington, DC 20036, U.S.A. Please remit $5.00 in advance for the microfiche.

TABLE 4. Atomic parameters: Amblygonite-montebrasite samples

		AF-47	AF-43	A-2	A-1	AF-46	M6116	AF-65
P	*x*	−0.01605(6)	−0.01576(8)	−0.01538(6)	−0.01496(7)	−0.01457(6)	−0.01308(8)	−0.01328(7)
	y	0.34212(4)	0.34196(6)	0.34136(4)	0.34095(5)	0.34047(5)	0.3319(6)	0.33910(5)
	z	0.26653(6)	0.26542(8)	0.26351(5)	0.26173(6)	0.26018(6)	0.25580(8)	0.25586(6)
	U(equiv.)*	41(2)	52(2)	54(1)	59(2)	57(2)	54(2)	56(2)
Al(1)	*x*	0	0	0	0	0	0	0
	y	0	0	0	0	0	0	0
	z	0	0	0	0	0	0	0
	U(equiv.)*	48(2)	58(3)	58(2)	60(3)	60(2)	56(2)	61(3)
Al(2)	*x*	0	0	0	0	0	0	0
	y	0	0	0	0	0	0	0
	z	1/2	1/2	1/2	1/2	1/2	1/2	1/2
	U(equiv.)*	46(2)	56(3)	55(2)	58(2)	57(2)	55(3)	57(2)
O(1)	*x*	−0.3172(2)	−0.3172(3)	−0.3169(2)	−0.3163(2)	−0.3160(2)	−0.3148(2)	−0.3152(2)
	y	0.0154(1)	0.0156(2)	0.0159(1)	0.0161(2)	0.0166(1)	0.0192(2)	0.0188(2)
	z	−0.1592(2)	−0.1579(2)	−0.1551(2)	−0.1523(2)	−0.1500(2)	−0.1426(2)	−0.1425(2)
	U(equiv.)*	66(4)	80(5)	84(3)	87(4)	86(4)	84(5)	87(4)
O(2)	*x*	0.2981(2)	0.2983(3)	0.2980(2)	0.2981(2)	0.2984(2)	0.2987(2)	0.2988(2)
	y	0.0581(1)	0.0584(2)	0.0589(1)	0.0594(2)	0.0597(1)	0.0609(2)	0.0606(2)
	z	0.5743(2)	0.5758(2)	0.5783(2)	0.5809(2)	0.5829(2)	0.5884(2)	0.5882(2)
	U(equiv.)*	65(4)	79(5)	87(3)	90(4)	90(4)	87(5)	90(4)
O(3)	*x*	0.1013(2)	0.1010(3)	0.1004(2)	0.1001(2)	0.0998(2)	0.0995(3)	0.0995(2)
	y	−0.2234(1)	−0.2236(2)	−0.2227(1)	−0.2224(2)	−0.2222(1)	−0.2209(2)	−0.2210(2)
	z	−0.3897(2)	−0.3895(2)	−0.3879(2)	−0.3868(2)	−0.3860(2)	−0.3830(2)	−0.3827(2)
	U(equiv.)*	63(4)	75(5)	79(3)	80(4)	81(4)	76(5)	82(4)
O(4)	*x*	0.0265(2)	0.0266(3)	0.0258(2)	0.0259(2)	0.0260(2)	0.0290(3)	0.0285(2)
	y	0.2362(1)	0.2357(2)	0.2346(1)	0.2340(2)	0.2332(1)	0.2320(2)	0.2317(2)
	z	0.1035(2)	0.1026(2)	0.0998(2)	0.0980(2)	0.0964(2)	0.0925(2)	0.0924(2)
	U(equiv.)*	76(4)	86(5)	94(4)	102(4)	101(4)	97(6)	97(4)
OH/F	*x*	0.0471(2)	0.0442(3)	0.0391(2)	0.0346(2)	0.0304(2)	0.0191(2)	0.0194(2)
	y	0.0890(1)	0.0882(2)	0.0871(1)	0.0859(1)	0.0850(1)	0.0824(2)	0.0828(1)
	z	−0.2265(2)	−0.2278(2)	−0.2306(2)	−0.2329(2)	−0.2352(2)	−0.2413(2)	−0.2410(2)
	U(equiv.)*	59(4)	79(5)	88(3)	93(4)	92(4)	98(5)	102(4)
Li	*x*	0.0696(5)	0.0687(8)	0.0663(6)	0.0617(7)	0.0579(7)	0.0514(11)	0.0503(8)
	y	−0.3202(4)	−0.3198(6)	−0.3209(4)	−0.3217(5)	−0.3220(5)	−0.3236(7)	−0.3221(5)
	z	0.3101(6)	0.3079(8)	0.3010(7)	0.2936(9)	0.2871(9)	0.2736(12)	0.2718(9)
	U(equiv.)*	172(12)	196(17)	259(13)	326(18)	351(18)	383(27)	367(21)
H	*x*	0.183(4)	0.178(4)	0.190(4)	—	—	—	—
	y	0.129(3)	0.132(3)	0.129(3)	—	—	—	—
	z	0.848(4)	0.850(4)	0.832(4)	—	—	—	—
	U(equiv.)*†	100	100	100				
				Split Li model				
Li(1)	*x*	0.07(5)	0.06(1)	0.05(1)	0.08(3)	0.05(1)	0.050(4)	0.0376(19)
	y	−0.32(5)	−0.318(9)	−0.33(1)	−0.32(2)	−0.315(6)	−0.320(3)	−0.3230(14)
	z	0.31(4)	0.285(5)	0.28(1)	0.28(3)	0.263(6)	0.2403(16)	0.242(3)
	U(equiv.)*	172(94)	118(90)	222(112)	277(166)	251(76)	201(1)	197(47)
Li(2)	*x*	0.07(5)	0.08(1)	0.08(1)	0.05(3)	0.061(9)	0.0654(19)	0.051(4)
	y	−0.32(5)	−0.322(9)	−0.31(1)	−0.32(2)	−0.329(7)	−0.3239(14)	−0.324(3)
	z	0.31(4)	0.331(5)	0.32(1)	0.31(3)	0.310(6)	0.3070(17)	0.301(3)
	U(equiv.)*	172(94)	118(90)	222(112)	277(116)	251(76)	201(1)	197(47)

* All *U* values are $\times 10^4$.
† Not refined.

atite contamination. The very minor Na contents of some amblygonite may also be due to contamination, as even at the scale of microprobe analysis (30 μm), none of the Na-bearing samples of this study was free of fine veins of lacroixite. In conclusion, the only significant variation in the chemistry of the amblygonite-montebrasite series is in the F/OH ratio.

Most of the samples examined show some slight variation in F/OH ratio within a single crystal. This variation does not seem to be systematic; there are equal numbers of samples showing F- or OH-enrichment toward crystal rims (Černá et al., 1973). Furthermore, the magnitude of intracrystalline variation of the F/OH ratio is slight compared to intercrystalline variations within a sample batch; indeed, the latter may range up to 30% (Table 1). In fact, this was the largest source of systematic error in the study: it proved difficult to separate fractions of batches of equal composition for the various experimental methods of investigation.

Sampling consistency is illustrated in Figure 2. Comparison of the F analyses given here with wet chemical analyses of F (Černá et al., 1973) shows that most data points are scattered closely about the expected 1/1 slope (Fig. 2a), indicating that the electron-microprobe results are accurate. The vertical bars in Figure 2a show intrasample variations in F content, as assessed by microprobe analysis. The bars show that the largest deviations from ideality in the plot can be explained as caused by

TABLE 5. Interatomic distances (Å) and angles (°) in crystals of amblygonite-montebrasite

		AF-47	AF-43	A-2	A-1	AF-46	M6116	AF-65
P-O(1)a		1.533(2)	1.532(2)	1.532(1)	1.534(2)	1.535(2)	1.535(2)	1.534(2)
P-O(2)b		1.530(1)	1.529(2)	1.530(1)	1.527(2)	1.527(1)	1.526(2)	1.527(2)
P-O(3)c		1.543(2)	1.545(2)	1.543(2)	1.543(2)	1.544(2)	1.548(2)	1.545(2)
P-O(4)		1.528(2)	1.528(2)	1.527(2)	1.525(2)	1.524(2)	1.526(2)	1.527(2)
⟨P-O⟩		1.534	1.534	1.533	1.532	1.533	1.534	1.533
O(1)a-O(2)b		2.415(2)	2.413(2)	2.411(2)	2.410(2)	2.409(2)	2.409(2)	2.406(1)
O(1)a-O(3)c		2.522(2)	2.520(3)	2.520(2)	2.521(2)	2.520(2)	2.519(2)	2.519(2)
O(1)a-O(4)		2.537(2)	2.538(3)	2.534(2)	2.533(3)	2.532(3)	2.530(2)	2.528(2)
O(2)b-O(3)c		2.516(2)	2.517(3)	2.521(2)	2.521(3)	2.524(2)	2.530(2)	2.529(2)
O(2)b-O(4)		2.498(2)	2.499(3)	2.505(2)	2.504(2)	2.507(2)	2.514(2)	2.517(2)
O(3)c-O(4)		2.530(3)	2.531(3)	2.522(3)	2.519(3)	2.517(3)	2.518(2)	2.518(2)
⟨O-O⟩P		2.503	2.503	2.502	2.501	2.502	2.503	2.503
O(1)a-P-O(3)b		104.1(1)	104.0(1)	103.9(1)	103.9(1)	103.7(1)	103.8(1)	103.6(1)
O(1)a-P-O(3)c		110.1(1)	110.0(1)	110.1(1)	110.0(1)	109.9(1)	109.6(1)	109.8(1)
O(1)a-P-O(4)		112.0(1)	112.1(1)	111.9(1)	111.8(1)	111.7(1)	111.5(1)	111.4(1)
O(2)b-P-O(3)c		110.0(1)	109.9(1)	110.3(1)	110.4(1)	110.5(1)	110.8(1)	110.8(1)
O(2)b-P-O(4)		109.6(1)	109.7(1)	110.1(1)	110.2(1)	110.5(1)	110.9(1)	111.0(1)
O(2)c-P-O(4)		110.9(1)	110.9(1)	110.5(1)	110.4(1)	110.3(1)	110.0(1)	110.1(1)
⟨O-P-O⟩		109.5	109.4	109.5	109.5	109.4	109.4	109.5
Al(1)-O(1)	×2	1.895(2)	1.894(2)	1.889(2)	1.881(2)	1.879(2)	1.868(2)	1.868(2)
Al(1)-O(4)	×2	1.916(2)	1.912(2)	1.901(2)	1.893(2)	1.887(2)	1.880(2)	1.876(2)
Al(1)-OH	×2	1.898(2)	1.892(2)	1.880(2)	1.871(2)	1.865(2)	1.846(2)	1.848(2)
⟨Al(1)-O⟩		1.899	1.890	1.882	1.877	1.865	1.864	1.864
O(1)-O(4)	×2	2.692(2)	2.690(3)	2.675(2)	2.664(2)	2.658(2)	2.645(2)	2.643(2)
O(1)-O(4)c	×2	2.698(2)	2.693(3)	2.684(2)	2.673(3)	2.667(3)	2.655(2)	2.651(2)
O(1)-OH	×2	2.745(3)	2.736(3)	2.717(3)	2.698(3)	2.685(3)	2.642(2)	2.649(2)
O(1)-OHc	×2	2.618(2)	2.617(3)	2.613(2)	2.607(2)	2.608(2)	2.610(2)	2.606(1)
O(4)-OH	×2	2.619(3)	2.612(3)	2.593(2)	2.581(3)	2.570(3)	2.548(2)	2.547(2)
O(4)-OHc	×2	2.774(3)	2.766(3)	2.752(2)	2.740(3)	2.733(2)	2.718(2)	2.716(2)
⟨O-O⟩Al(1)		2.691	2.686	2.672	2.661	2.654	2.636	2.635
O(1)-Al(1)-O(4)	×2	89.9(1)	89.9(1)	89.8(1)	89.8(1)	89.8(1)	89.8(1)	89.8(1)
O(1)-Al(1)-O(4)c	×2	90.1(1)	90.1(1)	90.2(1)	90.2(1)	90.2(1)	90.2(1)	90.2(1)
O(1)-Al(1)-OH	×2	92.7(1)	92.5(1)	92.2(1)	92.0(1)	91.7(1)	90.7(1)	90.9(1)
O(1)-Al(1)-OHc	×2	87.3(1)	87.5(1)	87.8(1)	88.0(1)	88.3(1)	89.3(1)	89.1(1)
O(4)-Al(1)-OH	×2	86.7(1)	86.7(1)	86.6(1)	86.6(1)	86.5(1)	86.3(1)	86.3(1)
O(4)-Al(1)-OHc	×2	93.3(1)	93.3(1)	93.4(1)	93.4(1)	93.5(1)	93.7(1)	93.7(1)
⟨O-Al(1)-O⟩		90.0	90.0	90.0	90.0	90.0	90.0	90.0
Al(2)-O(2)	×2	1.853(2)	1.853(2)	1.848(2)	1.844(2)	1.844(2)	1.839(2)	1.839(2)
Al(2)-O(3)c	×2	1.915(2)	1.915(2)	1.906(2)	1.901(2)	1.900(2)	1.893(2)	1.892(2)
Al(2)-OHc	×2	1.901(2)	1.896(2)	1.882(2)	1.872(2)	1.863(2)	1.843(2)	1.846(2)
⟨Al(2)-O⟩		1.890	1.888	1.879	1.872	1.869	1.858	1.859
O(2)-O(3)c	×2	2.584(2)	2.588(3)	2.585(2)	2.584(3)	2.588(2)	2.589(2)	2.585(2)
O(2)-O(3)f	×2	2.743(2)	2.740(3)	2.723(2)	2.712(2)	2.707(2)	2.689(2)	2.690(2)
O(2)-OHf	×2	2.659(3)	2.658(3)	2.647(3)	2.639(3)	2.636(3)	2.622(2)	2.627(2)
O(2)-OHc	×2	2.651(2)	2.645(3)	2.629(2)	2.617(2)	2.607(2)	2.585(1)	2.584(2)
O(3)c-OHf	×2	2.750(3)	2.748(3)	2.730(2)	2.718(3)	2.713(2)	2.694(2)	2.695(2)
O(3)c-OHc	×2	2.646(2)	2.640(3)	2.626(2)	2.618(2)	2.607(2)	2.588(2)	2.591(2)
⟨O-O⟩Al(2)		2.672	2.670	2.657	2.648	2.643	2.628	2.629
O(2)-Al(2)-O(3)c	×2	86.6(1)	86.7(1)	87.0(1)	87.2(1)	87.4(1)	87.8(1)	87.7(1)
O(2)-Al(2)-O(3)f	×2	93.4(1)	93.3(1)	93.0(1)	92.8(1)	92.6(1)	92.2(1)	92.3(1)
O(2)-Al(2)-OHf	×2	90.2(1)	90.3(1)	90.4(1)	90.5(1)	90.6(1)	90.8(1)	90.9(1)
O(2)-Al(2)-OHc	×2	89.8(1)	89.7(1)	89.6(1)	89.5(1)	89.4(1)	89.2(1)	89.1(1)
O(3)c-Al(2)-OHf	×2	92.2(1)	92.3(1)	92.2(1)	92.2(1)	92.3(1)	92.3(1)	92.3(1)
O(3)c-Al(2)-OHc	×2	87.8(1)	87.7(1)	87.8(1)	87.8(1)	87.7(1)	87.7(1)	87.7(1)
⟨O-Al(2)-O⟩		90.0	90.0	90.0	90.0	90.0	90.0	90.0
Li-O(1)d		2.086(3)	2.087(5)	2.077(3)	2.059(4)	2.049(4)	2.044(5)	2.042(5)
Li-O(2)e		2.077(3)	2.080(5)	2.081(4)	2.090(4)	2.103(4)	2.119(4)	2.129(5)
Li-O(3)f		2.131(4)	2.142(6)	2.193(5)	2.239(5)	2.276(6)	2.375(5)	2.383(7)
Li-O(3)g		2.022(4)	2.029(6)	2.038(4)	2.058(7)	2.077(5)	2.104(6)	2.107(6)
Li-O(4)c		2.759(4)	2.737(6)	2.671(5)	2.614(7)	2.562(6)	2.445(6)	2.436(7)
Li-OHc		1.958(3)	1.950(5)	1.941(3)	1.930(4)	1.920(4)	1.922(5)	1.905(4)
⟨Li-O⟩5		2.055	2.058	2.066	2.075	2.085	2.113	2.113
⟨Li-O⟩6		2.172	2.171	2.167	2.165	2.165	2.168	2.167
Li-Pk		2.630(4)	2.633(5)	2.630(4)	2.624(4)	2.627(4)	2.632(4)	2.640(4)
Li(1)-O(1)d		2.078(10)	2.080(15)	2.034(7)	2.018(8)	2.004(8)	1.986(11)	1.999(8)
Li(1)-O(2)e		2.116(10)	2.114(15)	2.139(7)	2.165(8)	2.190(8)	2.212(10)	2.209(8)
Li(1)-O(3)f		2.238(11)	2.245(17)	2.347(8)	2.418(10)	2.465(9)	2.560(12)	2.574(9)
Li(1)-O(3)g		2.004(11)	2.009(17)	2.056(8)	2.078(9)	2.112(8)	2.164(12)	2.141(8)
Li(1)-O(4)c		2.645(10)	2.628(16)	2.513(8)	2.427(9)	2.363(9)	2.253(12)	2.243(9)
Li(1)-OHc		1.933(10)	1.931(15)	1.917(8)	1.904(8)	1.893(8)	1.908(11)	1.902(8)
⟨Li(1)-O⟩5		2.074	2.076	2.099	2.117	2.112	2.105	2.099
⟨Li(1)-O⟩6		2.169	2.168	2.168	2.168	2.171	2.181	2.178
Li(2)-O(1)d		2.099(9)	2.101(14)	2.134(7)	2.118(8)	2.114(7)	2.122(10)	2.104(7)
Li(2)-O(2)e		2.040(10)	2.051(15)	2.037(7)	2.032(8)	2.036(8)	2.045(11)	2.068(8)
Li(2)-O(3)f		2.024(11)	2.040(16)	2.040(8)	2.063(9)	2.093(9)	2.062(12)	2.091(9)

TABLE 5.—*Continued*

	AF-47	AF-43	A-2	A-1	AF-46	M6116	AF-65
Li(2)-O(3)g	2.049(12)	2.055(17)	2.034(8)	2.053(9)	2.063(9)	2.192(13)	2.194(9)
Li(2)-O(4)c	2.877(10)	2.845(16)	2.831(8)	2.801(9)	2.758(9)	2.640(12)	2.631(9)
Li(2)-OHc	1.991(9)	1.975(15)	1.975(7)	1.973(8)	1.964(8)	1.957(11)	1.973(8)
⟨Li(2)-O⟩5	2.041	2.044	2.044	2.048	2.054	2.076	2.086
⟨Li(2)-O⟩6	2.180	2.178	2.175	2.173	2.171	2.170	2.177
Li(1)-Li(2)	0.24(2)	0.22(2)	0.33(1)	0.39(1)	0.41(1)	0.41(2)	0.41(1)
H-OHf	0.85(2)	0.85(2)	0.94(2)				
H-O(4)b	2.06(2)	2.08(2)	1.99(2)				
OHf-O(4)b	2.855(3)	2.875(3)	2.912(3)				
OHf-H-O(4)b	155(1)	154(1)	164(1)				

Note: a: $1/2 - x - 1, 1/2 - y, -z$; b: $1/2 - x, 1/2 - y, 1 - z$; c: $-x, -y, -z$; d: $1/2 - x - 1, 1/2 - y - 1, -z$; e: $1/2 - x, 1/2 - y - 1, 1 - z$; f: $x, y, z + 1$; g: $1/2 - x, 1/2 - y - 1, -z$.

errors in sampling technique, not errors in the electron-microprobe analysis. Most deviant data points lie below the 1/1 curve, and thus the cause for the deviations cannot be contamination of bulk samples with lacroixite, as this would displace the points above the curve. Figure 2b further illustrates this point. Here, F/(F + OH) by optical methods (Greiner and Bloss, 1987) is compared to F/(F + OH) by chemical methods. Although agreement between optical and bulk (wet) chemical methods is poor, the electron microprobe data show that most of the disagreement is probably due to intrasample variations in the F/OH ratio. Unlike Figure 2a, the most deviant wet chemistry data points lie above the 1/1 curve; lacroixite contamination in the samples used for optical measurements (particularly sample AF-65) may be partially responsible. As a consequence of the above sampling problems, averages of microprobe data were used in preference to wet chemical data in plots involving crystal structural data because the microprobe samples were extracted from the same subbatches as the samples used in structural analysis, (and because the microprobe data represent a larger data set). Wet chemical analyses were used in plots only when an electron microprobe analysis was not available.

In the case of sample M6116, the F/(F + OH) ratio obtained by microprobe analysis disagreed sufficiently with the results of the crystal-structure analysis to warrant microprobe analysis of the single crystal used for data collection. The F content of the sample was measured, giving 11.01 wt% (average of two analyses, assuming Li, Al, and P to be present in stoichiometric amounts), significantly different from the mean value of 13.06 wt% obtained from analysis of other crystals from this sample; this value was used for chemical-structural correlations, not the value given in Table 1.

Thus, there seems to be no significant substitution of any foreign components into the minerals of the amblygonite-montebrasite series. Conversely, even the single crystals can show considerable small-scale heterogeneity in OH/F ratio.

Alteration and intergrowth

This work has identified pervasive alteration (and intergrowth) of amblygonite-montebrasite by lacroixite as a typical feature of minerals of this series; this agrees with the findings of Fransolet (1989). Figure 3 shows the lacroixite veining typical of members of this series. In some areas, there seems to be some structural control, with long linear veins intersecting at ~60°; in other areas the veining seems irregular. The density of veining seems quite

TABLE 10. Bond-valence* tables for montebrasite (AF-47) and amblygonite (AF-65)

	P	Al(1)	Al(2)	Li	Li(1)	Li(2)	⟨Li⟩	Σ
				AF-47				
O(1)	1.274	$0.513_{\downarrow}^{\times 2}$		0.185	0.188	0.181	0.185	1.972
O(2)	1.285		$0.565_{\downarrow}^{\times 2}$	0.189	0.175	0.203	0.189	2.039
O(3)	1.239		$0.490_{\downarrow}^{\times 2}$	0.170	0.139	0.210	0.175	2.109
				0.210	0.218	0.199	0.209	
O(4)	1.292	$0.489_{\downarrow}^{\times 2}$		0.059	0.071	0.050	0.061	1.840
OH		$0.510_{\downarrow}^{\times 2}$	$0.506_{\downarrow}^{\times 2}$	0.240	0.253	0.224	0.239	1.256
Σ	5.090	3.024	3.122	1.053	1.044	1.067	1.056	
				AF-65				
O(1)	1.270	$0.546_{\downarrow}^{\times 2}$		0.202	0.220	0.179	0.200	2.018
O(2)	1.296		$0.584_{\downarrow}^{\times 2}$	0.171	0.147	0.192	0.170	2.051
O(3)	1.232		$0.517_{\downarrow}^{\times 2}$	0.108	0.079	0.184	0.132	2.035
				0.178	0.167	0.151	0.159	
O(4)	1.296	$0.536_{\downarrow}^{\times 2}$		0.099	0.138	0.072	0.105	1.931
F		$0.447_{\downarrow}^{\times 2}$	$0.449_{\downarrow}^{\times 2}$	0.217	0.219	0.190	0.205	1.113
Σ	5.094	3.058	3.100	0.975	1.021	1.010	1.017	

* Calculated from the curves of Brown (1981).

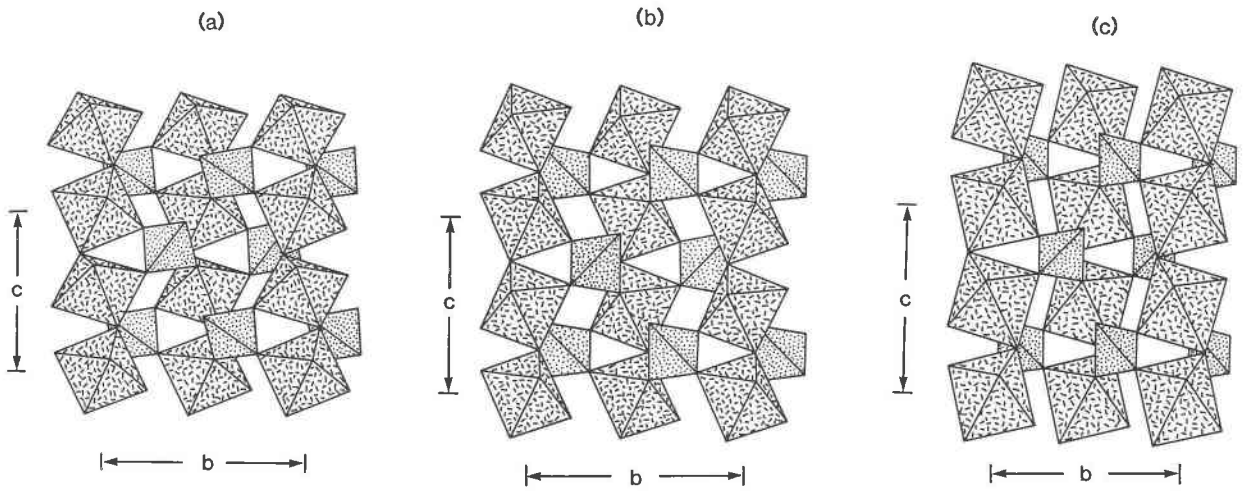

Fig. 1. The structures of (**a**) amblygonite-montebrasite, compared with the structures of (**b**) titanite and (**c**) kieserite; tetrahedra are dotted, octahedra are dashed.

variable across the crystal, suggestive of postcrystallization Na metasomatism that is sometimes controlled by cleavage. Conversely, Fransolet (1989) records textures much more reminiscent of exsolution, as well as obvious associations of montebrasite and lacroixite caused by alteration. A study of the phase equilibria for the montebrasite-lacroixite join is desirable.

Bond-length variations

The ⟨P-O⟩ distances are constant across the series at a typical value of 1.533 Å. Individual P-O distances show only very minor change with compositional variation (Fig. 4a), in agreement with the general idea that the more tightly bonded an anionic group, the less susceptible it is to inductive effects in a structure. Conversely, there is significant change in O-P-O bond angles across the series (Fig. 4b). All changes are linear with composition; four of the angles decrease slightly with increasing F/(F + OH), and the remaining two [O(2)b-P-O(3)c and O(2)b-P-O(4)] increase significantly with increasing F/(F + OH), the ⟨O-P-O⟩ being constant across the series.

There are two crystallographically distinct $AlO_4(OH,F)_2$ octahedra in the structure, both of which have a *trans* arrangement of the two monovalent anions. The ⟨Al-ϕ⟩ (ϕ: unspecified ligand) distances decrease linearly with increasing F across the series (Fig. 4c). Extrapolating to a

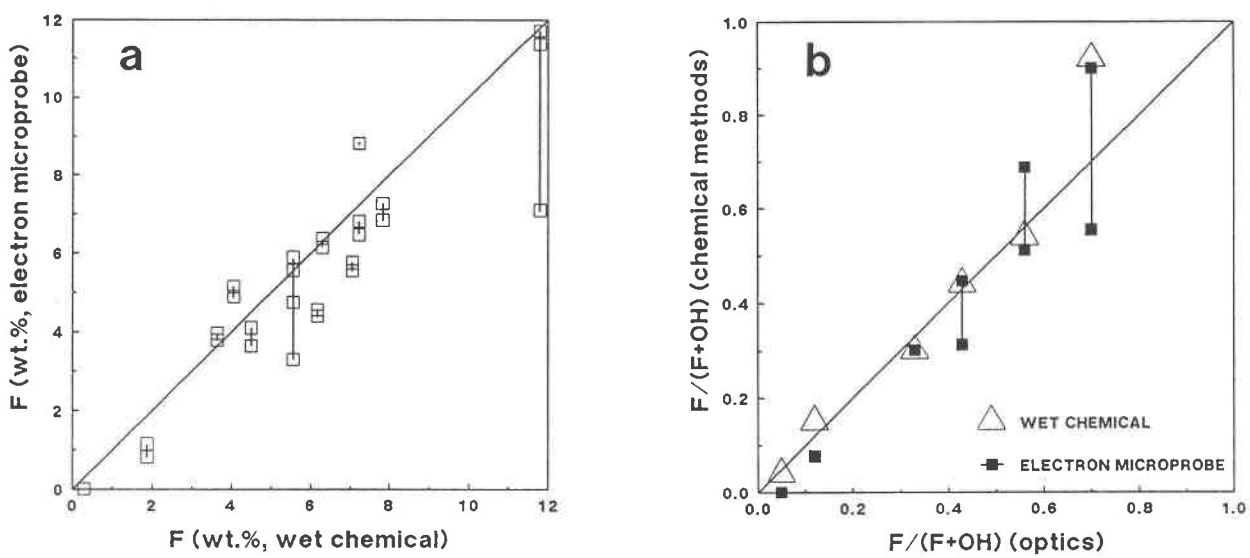

Fig. 2. Comparison of F compositions of samples of amblygonite-montebrasite determined by different methods: (**a**) electron microprobe vs. wet chemical results for wt% F; (**b**) F/(F + OH) determined by chemical methods vs. F/(F + OH) determined from optics. The line through the data shows the 1:1 relationship and is not a regression line; the vertical bars represent the range in composition of the microprobe analyses.

F-free end-member gives a grand $\langle Al\text{-}O_4(OH)_2\rangle$ distance of 1.896 Å; this compares with a constituent ionic radii sum of 1.892 Å (radii from Shannon, 1976), in fairly good agreement. Extrapolation to the F end-member gives a grand $\langle Al\text{-}O_4F_2\rangle$ bond length of 1.855 Å, as compared with a constituent ionic radii sum of 1.879 Å. Thus with increasing substitution of F for OH, the $\langle Al\text{-}\phi\rangle$ distances contract more rapidly than a hard-sphere model would suggest.

Figure 4d shows the variation in individual Li-ϕ distances across the series for the unsplit Li position. For the (OH)-rich members, it seems reasonable to designate the Li as five-coordinate. However, at the F-rich end of the series, this is obviously not tenable, as Li-O(3)f and Li-O(4)c bond lengths have converged to nearly the same value; hence the Li is either four-coordinate or six-coordinate. We can understand this trend in terms of the substitution of (OH) by F, and the local bond-valence requirements around O(4) in the structure. Table 10 shows empirical bond-valence calculations for samples AF-47 [F/(F + OH) = 0.04] and AF-65 [F/(F + OH) = 0.90]. In the OH-rich member, the Li-O(4) bond is (weak to) nonexistent, and the H bond from OH to O(4) (Fig. 5) plays an important role in satisfying the bond-valence requirements of the O(4) anion. In the F-rich member, there is no significant OH in the structure, and hence O(4) needs additional bond-valence from elsewhere to satisfy its requirements. It is apparent from Table 10 that this comes primarily from the shortening of the Al(1)-O(4) and Li-O(4) distances to the point at which they contribute sufficient additional bond-valence towards the local satisfaction of the O(4) anion to compensate for the loss of the H bond. The gradual change from five-coordination at one end of this series to six-coordination at the other is also instructive in terms of the arguments that sometimes arise about the most appropriate coordination number in specific crystals. As is apparent here, there does not seem to be a specific break between the two coordination numbers; they grade imperceptibly into one another. For five-coordinate Li, there is a very significant increase in $\langle Li\text{-}\phi\rangle$ across the series (Fig. 4e), for six-coordination, the $\langle Li\text{-}\phi\rangle$ distance decreases slightly across the series; such relationships could be taken to favor six-coordination over five-coordination if one wished to assign a specific coordination to Li.

An additional complication with regard to the Li is that a distinct splitting occurs, the amount of which is dependent upon composition. In Figure 4f, it can be seen that a small amount of splitting (0.21 Å) occurs at the OH-rich end, gradually increasing to about 0.41 Å around F/(F + OH) ≈ 0.50, and remaining constant across the F-dominant range of the series. Unfortunately, we do not know the exact behavior of such splitting with composition, as we have no end-member compositions to examine. Possibly the splitting falls to zero at one or both of the end-member compositions; however, more likely is the behavior suggested in Figure 4f, in which the splitting is a characteristic of all compositions. Figures 4g and 4h show the individual bond lengths as a function of composition for the two split-Li sites, designated Li(1) and Li(2) respectively. The behavior of these two sites as a function of composition is entirely different. Li(1) seems to be five-coordinate at the OH end, becomes six- (or possibly four-) coordinate at intermediate compositions, and reverts to five-coordination again, but with a different set of ligands compared to its coordination at the other end of the series. Conversely, Li(2) is five-coordinate all the way across the series. It is tempting to ascribe the splitting of the Li position to local bond-valence requirements, but the splitting seems to make no significant difference to the bond-valence sums around the anions or around the cations (Table 10).

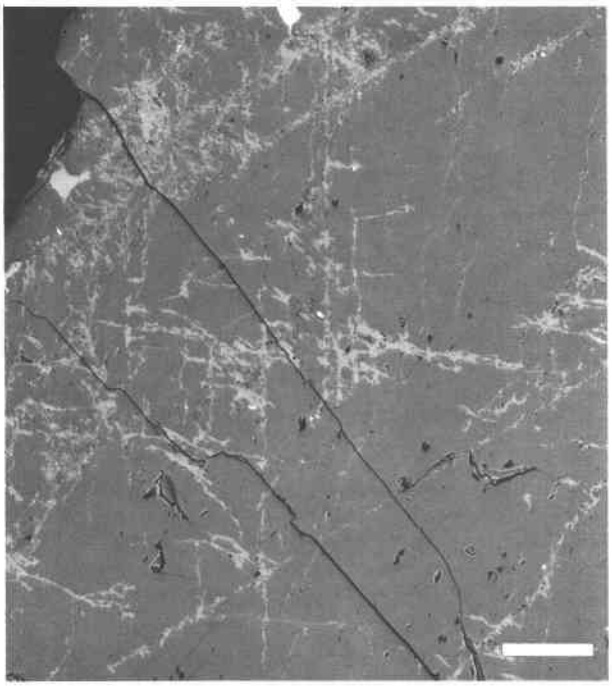

Fig. 3. Backscattered electron image of sample AF-65, showing the pervasive veining of montebrasite by lacroixite; the length of the scale bar is 20 μm.

MAS-NMR spectra

^{31}P spectra. There is one broad ^{31}P peak at −15.8 ppm (Fig. 6a) with a peak width of 340–410 Hz that remains constant across the series, consistent with the constant (PO_4) tetrahedral geometry (Table 5, Fig. 4a). The higher-field chemical shift of amblygonite compared to hydroxylapatite and fluorapatite at 2.8 ppm (Rothwell et al., 1980) can be related to the shorter mean P-O distances in amblygonite as compared with apatite (Bleam et al., 1989). This in turn relates to the difference in coordination of the anions of the phosphate groups. In the amblygonite-montebrasite series, the anions of the phosphate group have a mean coordination number of 3.25; in apatite, the anions of the phosphate group have a mean

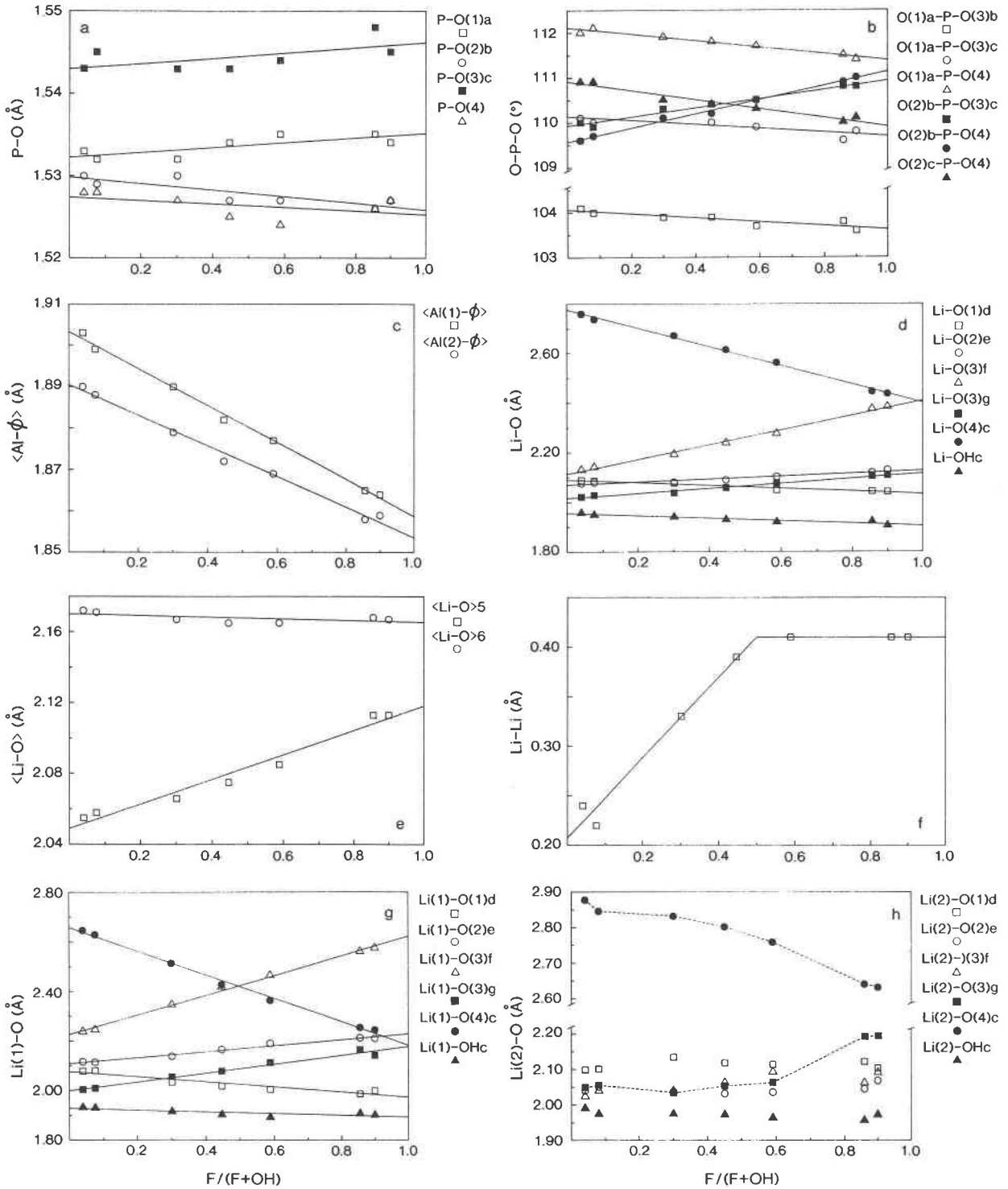

Fig. 4. Variation in structural parameters as a function of F/(F + OH): (**a**) P-O distances; (**b**) O-P-O angles; (**c**) ⟨Al(1)-ϕ⟩ and ⟨Al(2)-ϕ⟩ distances; (**d**) Li-O distances; (**e**) ⟨Li-O⟩ distances for five- and six-coordinations; (**f**) Li(1)-Li(2) separations; (**g**) Li(1)-O distances; (**h**) Li(2)-O distances.

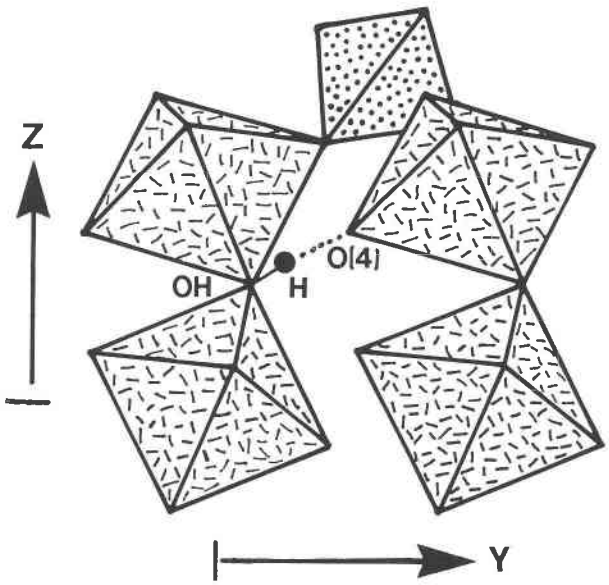

Fig. 5. H bonding arrangement in montebrasite.

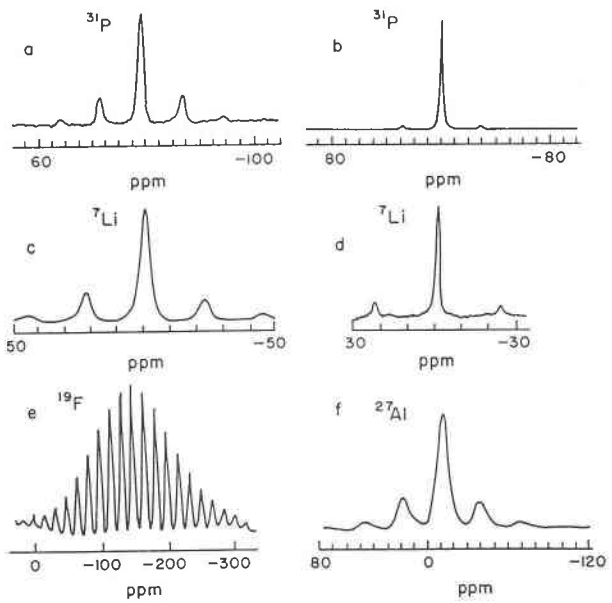

Fig. 6. Typical MAS-NMR spectra for samples of amblygonite-montebrasite: **(a)** ^{31}P in amblygonite; **(b)** ^{31}P in fluorapatite, for comparison; (c) ^{7}Li in amblygonite; **(d)** ^{7}Li in spodumene, for comparison; **(e)** ^{19}F spectrum, with strong spinning sidebands; **(f)** ^{27}Al spectrum.

coordination number of 4.0. The ^{31}P spectra of amblygonite has higher spinning sideband intensity than apatite (Fig. 6b), indicating higher chemical-shift anisotropy or asymmetry of the PO_4 tetrahedron (Herzfeld and Berger, 1980; Maricq and Waugh, 1980).

^{7}Li Spectra. Li occupies a cavity surrounded by six anions in a distorted octahedral arrangement; five of the anions are O^{2-} belonging to (PO_4) groups, and the sixth anion is OH^- or F^-. The octahedron itself is reasonably regular, but because the Li occupies an off-centered (split) position, the environment of the Li is extremely asymmetric. This is apparent in the high intensity of the spinning sidebands in the ^{7}Li spectrum (Fig. 6c). This can be compared with the low intensity spinning sidebands in the ^{7}Li spectrum of spodumene (Fig. 6d), in which the Li occupies a much more central position in its coordination polyhedron.

The ^{7}Li peaks of the amblygonite-montebrasite series are nearly three times as broad as the corresponding peaks of spodumene (Figs. 6c and 6d). There are two possible causes for this difference: (1) the higher asymmetry of the environment in members of the amblygonite-montebrasite series could enhance quadrupolar broadening relative to that in spodumene; (2) there is more than one peak (closely overlapping) in the spectra of the amblygonite-montebrasite series. The first possibility was tested in the following manner. As quadrupolar effects are reduced at higher field, we recorded a ^{7}Li amblygonite spectrum at 77.7 MHz and 155.5 MHz. The signals were approximately 100 Hz narrower at lower field, and thus the broadening cannot be due to quadrupolar effects. The separation between peaks usually increases at higher field, suggesting that the additional broadening of peaks of the amblygonite spectra (relative to that of spodumene) is due to the presence of multiple overlapping peaks. The only chemical change across the series involves the OH $\rightleftharpoons$ F substitution, which correlates with a slight shift of peak position to higher field. This also means that there is short-range anion variability around the Li site. This is further complicated by the fact that Li occupies two different off-center environments [labeled Li(1) and Li(2) in Tables 4 and 5]. We do not know whether local OH-F occupancy correlates with Li(1)/Li(2) occupancy. Nevertheless, the structural data show that Li occurs in a variety of (locally) different environments. The range of chemical shift for ^{7}Li is generally rather narrow (a few ppm only) and hence it is not surprising that peaks from fairly similar environments should not be well resolved.

^{6}Li spectra. The ^{6}Li spectra have the same chemical shift but are narrower than those of ^{7}Li, which could be due to the smaller quadrupolar moment of ^{6}Li compared to ^{7}Li. Separate peaks were not resolved, but the smaller peak width could also be attributed to unresolved peaks being less spread out at the lower field strength used for the ^{6}Li spectra. The signal-to-noise ratio is less because of the sensitivity of ^{6}Li being 3×10^{-4} that of ^{7}Li.

^{19}F spectra. The ^{19}F MAS-NMR spectra (Fig. 6e) consist of one very broad absorption at -146 ± 1 ppm with intense spinning sidebands, the first set of spinning sidebands having the same intensity as the main peak. There is no variation in spectra with chemical composition. The intensity of the sidebands may be related to the threefold coordination of the F site, as the ^{19}F spectrum of fluorapatite (in which fluorine is similarly coordinated) also shows intense sidebands (Yesinowski and Mobley,

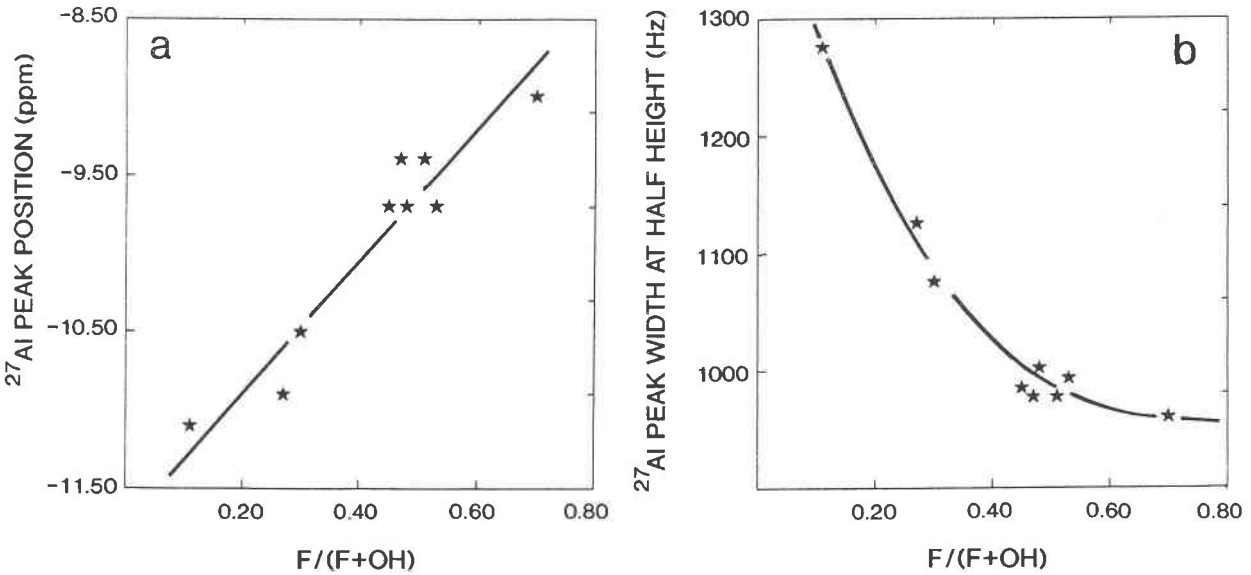

Fig. 7. (**a**) Variation in ^{27}Al peak position as a function of F/(F + OH) across the amblygonite-montebrasite series; (**b**) variation in ^{27}Al peak width as a function of F/(F + OH) across the amblygonite-montebrasite series.

1983). The ^{19}F spinning sidebands of amblygonite are more intense than those of apatite because the F site is more asymmetric; in amblygonite, F is bonded to two Al and one Li atoms, whereas in apatite, F is bonded to three Ca atoms. In the ^{19}F spectra of amphiboles, the intensity of the spinning sidebands is much less, and differences among sideband intensities have been interpreted as an indication of differing site asymmetries (Raudsepp et al., 1987). The chemical shift of the more shielded ^{19}F nucleus of amblygonite (with Al and Li at distances of 1.91 and 1.93 Å, respectively) is to the high-field side of the value −99.5 ppm for fluorapatite (with Ca-F distances of 2.36 Å).

^{27}Al spectra. There are two Al sites in amblygonite, both octahedrally coordinated by 4 O and 2 OH or F in a *trans* arrangement. There is 0.01 Å difference in the mean bond length of the Al(1) and Al(2) octahedra, indicating some difference in the degree of average covalency of the bonds to each constituent cation. Thus one might expect two principal signals in the NMR spectrum caused by ^{27}Al at each of the two sites. However, ^{27}Al has nuclear spin of 5/2 and thus possesses a quadrupole moment that leads to considerable line broadening when compared to spin 1/2 nuclei such as ^{29}Si. Consequently we see a rather broad single peak (Fig. 6f) that is the result of overlap of two quadrupolar line-broadened signals.

As the F/(F + OH) ratio increases, the ^{27}Al peak shifts to lower field (Fig. 7a). This indicates a slight decrease in the covalency of the bonding at the two Al sites owing to the gradual replacement of (OH) by the more electronegative F. The width of the absorption also decreases with increasing F/(F + OH) (Fig. 7b). This could be caused by increased overlap of the two peaks with increasing F content; however, the details of the bond geometry across the series do not exhibit sufficient differential change to suggest that this is the case. More probably there is less line broadening in both peaks due to the average decrease in dipolar coupling between the proton and the Al with decreasing (OH) content.

Infrared spectra

The powder infrared spectra in the principal O-H stretching region for the various samples are shown in Figure 8. In the most OH-rich sample, there is a strong peak in the principal O-H stretching regions at 3390 cm^{-1}, with a half-width of about 50 cm^{-1}. This is indicative of a fairly strong H bond, in agreement with the H bond valence assigned in the empirical bond-valence table (Table 10). With increasing F/(F + OH), the peak becomes weaker and broader, and shifts to lower wavenumbers. Each of these features can be explained by the substitution of F for OH in the structure. With increasing substitution, OH is replaced by F, and thus the total absorption (per unit of sample) becomes less. With increasing substitution of OH for F, there is increasing local (short-range) disorder in the structure, causing a wider variety of OH environments and hence a broader, more ill-defined OH absorption. Lastly, with substitution of a F ion for an OH ion, there is local loss of bond valence owing to the loss of one H bond, and the remaining H bonds thus become stronger to accommodate this loss. Hence there should be a gradual shift of principal stretching frequencies to lower wavenumbers with decreasing numerical frequency of H bonds, as is observed.

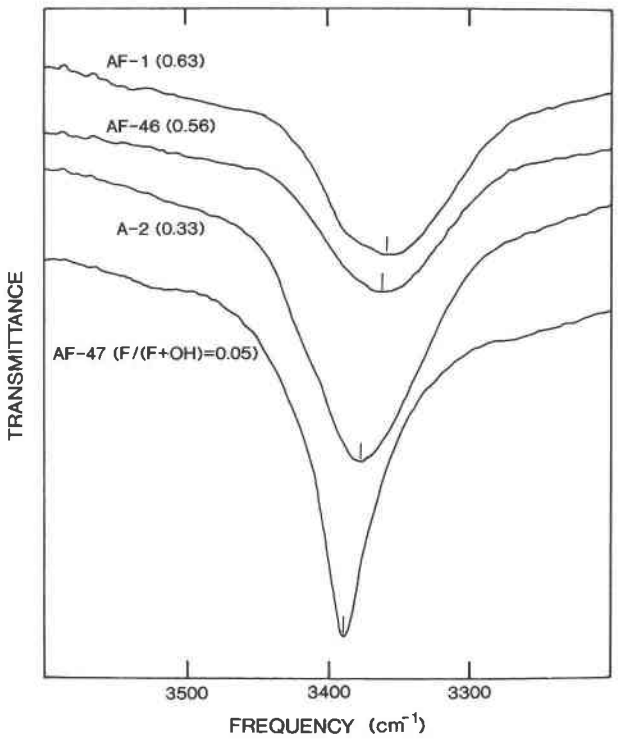

Fig. 8. Infrared spectra in the principal O-H stretching region for selected compositions across the amblygonite-montebrasite series.

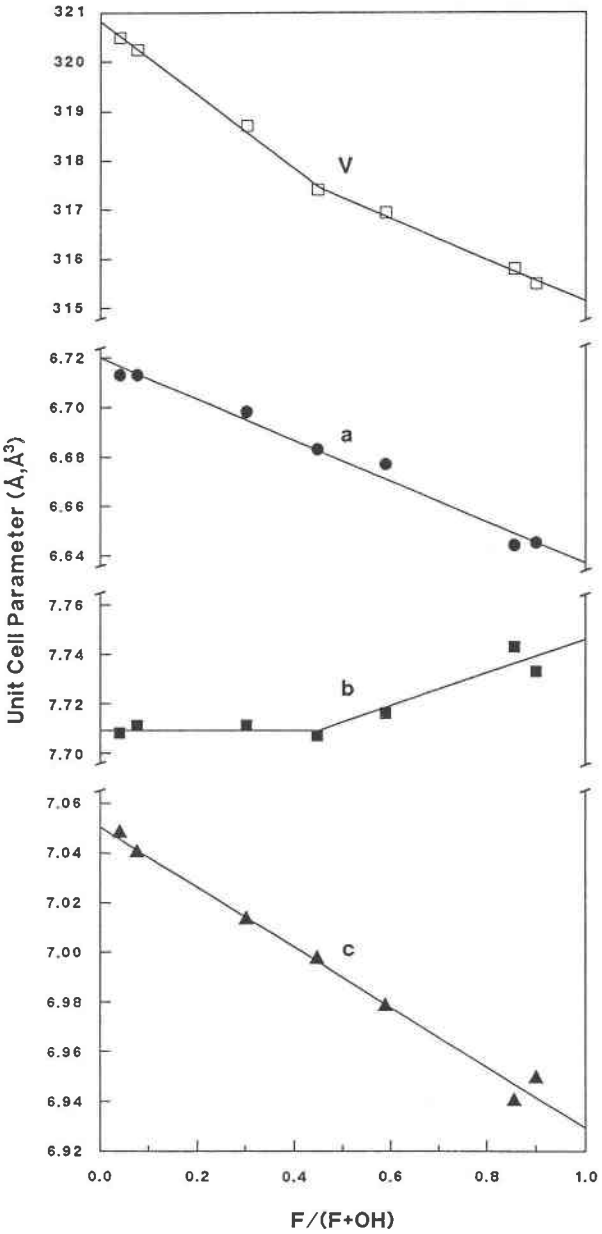

Fig. 9. Variation in selected cell dimensions as a function of F/(F + OH) across the amblygonite-montebrasite series.

Sample AF-1

As briefly outlined in the experimental section, the structure refinement for this particular sample was not straightforward. The variation in cell volumes for the nine crystals selected from this sample suggests considerable grain-to-grain heterogeneity, and the difficulties encountered in the four refinements for this sample indicate significant compositional heterogeneity even within single grains. First, the high R indices obtained for the refinements contrasted strongly with the values obtained for the rest of the samples ($R \approx 2\%$). Second, slow scans across the diffraction maxima showed asymmetric peaks with pronounced shoulders. Both of these factors suggest multiphase material on a fairly coarse scale. Incoherent scattering from two phases of different composition would result in higher R indices. Different proportions of the two phases would account for the grain-to-grain heterogeneities observed in the measured cell dimensions. If this is the case, there are two possibilities. (1) There is incomplete secondary alteration of primary amblygonite, resulting in two (or more) phases of different compositions. (2) There is immiscibility in the region of F/(F + OH) $\approx$ 0.70, resulting in two phases of different compositions. The continuous linear variation in structural parameters across the series does not suggest immiscibility. Detailed microprobe analysis showed extensive alteration in AF-1, and also revealed that alteration and intergrowth are very common in samples of amblygonite-montebrasite, even in material that appears to be of gem quality.

Solid solution across the series

Previous work has assumed that there is complete solid solution across the amblygonite-montebrasite series, with cell parameters and refractive indices linearly related to F/OH composition. The work presented here, together with that of Greiner (1986) and Greiner and Bloss (1987), suggests that the situation is more complex. Let us consider first the variation in cell dimensions (Fig. 9). The cell volume decreases monotonically with increasing F $\rightleftharpoons$

TABLE 11. Minerals structurally related to amblygonite-montebrasite

Mineral	Formula	a(Å)	b(Å)	c(Å)	β(°)	Space group	Reference
Dwornikite	$[Ni(SO_4)(H_2O)]$	6.839	7.582	7.474	117.85	$C2/c$	(1)
Gunningite	$[Zn(SO_4)(H_2O)]$	6.954(8)	7.586(8)	7.566(8)	115.93(3)	$C2/c$	(2)
Kieserite	$[Mg(SO_4)(H_2O)]$	6.912(2)	7.624(2)	7.642(2)	117.70(2)	$C2/c$	(3)
Poitevinite	$[Cu(SO_4)(H_2O)]$	7.176(10)	7.426(10)	7.635(10)	116.15(3)	$C2/c$	(2)
Szmikite	$[Mn(SO_4)(H_2O)]$	7.120(1)	7.666(1)	7.766(1)	115.85(1)	$C2/c$	(4)
Szomolnokite	$[Fe^{2+}(SO_4)(H_2O)]$	7.123	7.468	7.624	115.9	$C2/c$	(1)
Durangite	$Na[Al(AsO_4)F]$	6.574(1)	8.505(2)	7.019(1)	115.34	$C2/c$	(5)
Isokite	$Ca[Mg(PO_4)F]$	6.52(5)	8.75(5)	7.16	109.8	$C2/c$	(6)
Lacroixite	$Na[Al(PO_4)F]$	6.414	8.207	6.885	115.47	$C2/c$	(7)
Malayaite	$Ca[Sn(SiO_4)O]$	6.668(4)	8.895(9)	7.156(6)	113.4(1)	$C2/c$	(8)
Panasqueiraite	$Ca[Mg(PO_4)OH]$	6.535(3)	8.753(4)	6.919(4)	112.33(4)	$C2/c$	(6)
Tilasite	$Ca[Mg(AsO_4)]F$	6.688(2)	8.944(2)	7.560(2)	121.16(2)	$C2/c$	(9)
Titanite $P2_1/c$	$Ca[Ti(SiO_4)O]$	6.562(1)	8.714(3)	7.068(1)	113.82	$P2_1/c$	(10)
Titanite $C2/c$	$Ca[(Ti, Al, Fe^{3+})(SiO_4)O]$	6.555(2)	8.718(5)	7.073(4)	113.97(5)	$C2/c$	(11)
Amblygonite*	$Li[Al(PO_4)F]$	6.6452(9)	7.733(1)	6.9193(6)	117.44(1)	$C\bar{1}$	(12)
Montebrasite**	$Li[Al(PO_4)OH]$	6.713(1)	7.708(1)	7.0194(7)	117.93(1)	$C\bar{1}$	(12)
Natromontebrasite	$Na[Al(PO_4)(OH)]$	—	—	—	—		
Tavorite†	$Li[Fe^{3+}(PO_4)OH]$	6.887(3)	7.907(3)	7.279(2)	117.79(3)	$C\bar{1}$	(12)

Note: References: (1) Pistorius (1960); (2) Pistorius (1961a); (3) Hawthorne et al. (1987); (4) Pistorius (1961b); (5) Foord et al. (1985); (6) Isaacs and Peacor (1981); (7) Pajunen and Lahti (1985); (8) Higgins and Ribbe (1977); (9) Bladh et al. (1972); (10) Taylor and Brown (1976); (11) Mongiorgi and Riva di Sanseverino (1968); (12) This study.

* $\alpha = 90.35(1)$, $\gamma = 91.20(1)°$.

** $\alpha = 91.31(1)$, $\gamma = 91.77(1)°$.

† $\alpha = 91.33(3)$, $\gamma = 92.51(4)$.

OH substitution, but the relationship is distinctly nonlinear (Fig. 9); this can also be seen in the analogous graph presented by Černá et al. (1973, Fig. 9). With regard to the individual axes, a and c decrease linearly with decreasing F/(F + OH), whereas b increases nonlinearly with decreasing F/(F + OH). It is not clear whether the latter variation is curved or is in two linear segments with a break at about F/(F + OH) = 0.50; however, we note that this break does occur at the composition at which there is a break in the Li(1)-Li(2) split-site separation (Fig. 4f).

It is notable that the optical properties measured by Greiner and Bloss (1987) also show nonlinear behavior as a function of composition. Moreover, this nonlinear behavior parallels that shown by the cell volume (Fig. 9), both showing negative deviations from linear behavior. This suggests that the nonlinearity in the optical data stems from the nonlinearity in the cell volume that propagates through the Gladstone-Dale relationship. This was tested in the following manner. A linear regression was carried out on the four most F-poor samples as a function of F/(F + OH) ratio; cell volumes were then calculated from this model for the three F-rich crystals used in this study. The mean refractive indices for these three crystals were then calculated from the predictive nonlinear models of Greiner and Bloss (1987). If these values are then corrected for the nonlinear variation in cell volumes noted above, the mean refractive indices then become linear with those of the rest of the series (Greiner and Bloss, 1987, Fig. 3). This shows that the nonlinear variation in refractive indices as a function of composition arises as a result of the analogous nonlinear behavior in the cell volume.

Solid solution of other components

As outlined above, the members of the amblygonite-montebrasite series examined here contain no significant substituents in addition to their principal components; previous analyses indicating significant other components (particularly Na and Ca) are most probably due to inclusions of apatite and veining by lacroixite. The question that arises from this observation is why these minerals do not incorporate minor amounts of other cations into their structures. The heteropolyhedral framework of the structure is topologically identical to those of titanite and kieserite (Fig. 1), both of which incorporate significant additional components into their structures; this is particularly the case for titanite (Higgins and Ribbe, 1976; Groat et al., 1985; Paul et al., 1981), in which there is significant substitution at every cation site in the structure. A compilation of the relevant minerals is given in Table 11.

We first examine the alkali and alkaline-earth cation sites. In titanite and minerals isostructural with it, this site is coordinated by seven anions, all of which bond to the central cation (Table 12). The arrangement is flexible enough to incorporate monovalent to trivalent cations, provided they are fairly large. In the amblygonite-montebrasite series, the analogous site is coordinated by six anions in octahedral coordination. Adjacent octahedral vertex-sharing chains have considerably different relative positions. The anion corresponding to the seventh coordination anion in titanite is 3.26 Å from the central cation (Li); to bring this anion back into a conformation similar to that in titanite would require cooperative movement of a large number of atoms with the chains assuming the same relative positions as in titanite. Presumably, such a local perturbation in the amblygonite-montebrasite structure is unacceptably large, and any substituent must therefore be six-coordinated; this means that the cavity is intrinsically smaller than in titanite. Although the ionic radius of a cation is a function of its coordination number, the decrease in radius from seven-

TABLE 12. Comparison of the alkaline earth and alkali cation coordinations in titanite and amblygonite

Titanite		Amblygonite	
Ca-O(1)a	2.286(6) (Å)	Li-Fh	1.905(4) (Å)
Ca-O(2)b	2.431(5)	Li-O(1)i	2.042(5)
Ca-O(2)c	2.431(5)	Li-O(2)j	2.129(5)
Ca-O(3)d	2.655(5)	Li-O(3)k	2.383(7)
Ca-O(3)e	2.655(5)	Li-O(4)h	2.436(7)
Ca-O(3)f	2.433(4)	Li-O(3)l	2.107(6)
Ca-O(3)g	2.433(5)	Li-O(3)m	[3.262(7)]

Note: a: $\bar{x}$, $1 - y$, $1 - z$; b: $\bar{x}$, $\bar{y}$, $1 - z$; c: x, $\bar{y}$, $\frac{1}{2} + z$; d: x, y, $1 + z$; e: $\frac{1}{2} - x$, y, $1 - z$; f: $\bar{x}$, y, $\frac{1}{2} - z$; g: $-\frac{1}{2} + x$, y, $\frac{1}{2} + z$; h: $\bar{x}$, $\bar{y}$, $\bar{z}$; i: $-\frac{1}{2} - x$, $-\frac{1}{2} - y$, $\bar{z}$; j: $\frac{1}{2} - x$, $-\frac{1}{2} - y$, $1 - z$; k: x, y, $1 + z$; l: $\frac{1}{2} - x$, $-\frac{1}{2} - y$, $\bar{z}$; m: $-\frac{1}{2} + x$, $-\frac{1}{2} + y$, z.

to six-coordination is not sufficient to compensate for the decrease in size of the interchain cavity. Thus, typical mean bond lengths for ($Ca\phi_6$) and ($Na\phi_6$) octahedra are 2.42 and 2.48 Å, respectively, compared with the interchain octahedral distance of ~2.17 Å in members of the amblygonite-montebrasite series. Again, this suggests that the local perturbation would be too great to incorporate Ca or Na at the Li site in amblygonite. For Na, this conforms with the observations that lacroixite ($NaAlPO_4F$), the Na analog of amblygonite, is monoclinic. Natromontebrasite, $NaAlPO_4OH$, is supposedly triclinic (Fleischer, 1987), but there is no X-ray evidence on this point, and we think it improbable that this is the case.

The situation is less clear for the Al sites. In titanite and kieserite, there is wide substitution at the analogous sites, specifically Sn^{4+}, Al, Mg, Ta^{5+}, Nb^{5+}, $Fe^{3+} \rightleftharpoons Ti$, and Fe^{2+}, Mn, Ni, Zn $\rightleftharpoons$ Mg, respectively. Despite the fact that tavorite, $NaFe^{3+}PO_4OH$, is isostructural with montebrasite, there seems to be no $Fe^{3+} \rightleftharpoons$ Al substitution in the natural minerals. Possibly this is caused by geochemical constraints: there is little or no Fe available at the time of crystallization of amblygonite-montebrasite, which tends to be an early primary phosphate. This not the case for other potential substituents (Sn^{4+}, Ta^{5+}, Nb^{5+}, Mg); their lack of incorporation can be ascribed to the fact that they all differ in valence from Al, and hence require coupled substitutions. Substitution of Mg for Al would require substitutions of Ca or Mg for Li. The former does not occur for the reasons discussed above; the latter needs more detailed consideration, as the cavity around the Li site seems an appropriate size for Mg incorporation. Replacing Al and Li by Mg (producing Mg_2PO_4F, the formula of wagnerite) results in quite a reasonable bond-strength distribution. Some distortions from ideal polyhedral geometry are required to satisfy local bond-valence requirements, but these are fairly small, and the reason for the lack of this particular substitution is not at all clear.

Thus although the structure of members of the amblygonite-montebrasite series is topologically identical with the titanite and kieserite structures, the lack of both solid solution and incorporation of other minor components can be seen to be a result of the different disposition of the [$M(TO_4)\phi_3$] octahedral-tetrahedral chains. In titanite and its isotypes, the seven-coordinated interchain site can admit a wide variety of cations of slightly different radius and charge without perturbing the disposition of the chains. Conversely, in members of the amblygonite-montebrasite series, the six-coordinated interchain site cannot incorporate other alkali or alkaline-earth cations without large local rearrangement of the chains, totally inhibiting such substitutions.

ACKNOWLEDGMENTS

We thank Petr Černý (University of Manitoba) for donating the samples, and Dan Greiner and Don Bloss (Virginia Polytechnic Institute) for cooperative work and discussion during the course of this project. Most of the NMR work was done at the South Western Ontario High Field NMR Centre (University of Guelph), and we thank R.E. Lenkinski and W. Klimstra for their assistance. We also thank J.A. Ripmeester (National Research Council, Ottawa) for the use of his MSL-300 NMR spectrometer to obtain ^6Li spectra, and for helpful discussion. Constructive and useful reviews were given by Don Bloss and Subrata Ghose. Financial support for this work was provided by the Natural Sciences and Engineering Council of Canada in the form of Graduate Scholarships to L.A.G. and B.L.S., a University Research Fellowship to F.C.H., Operating Grants to F.C.H. and J.S.H., and a major equipment grant and an Infrastructure Grant to F.C.H.

REFERENCES CITED

Baur, W.H. (1959a) Über Kristallstrukturelle Beziehungen zwischen Amblygonit, Kieserit und Titanit. Beiträge zur Mineralogie und Petrologie 6, 399–404.

——— (1959b) Die Kristallstruktur des Edelamblygonits $LiAlPO_4(OH,F)$. Acta Crystallographica, 12, 988–994.

Bladh, K.W., Corbett, R.K., McLean, W.J., and Laughon, R.B. (1972) The crystal structure of tilasite. American Mineralogist, 57, 1880–1884.

Bleam, W.F., Pfeffer, P.E., and Frye, J.S. (1989) ^{31}P solid state nuclear magnetic resonance spectroscopy of Al phosphate minerals. Physics and Chemistry of Minerals, 16, 455–464.

Brown, I.D. (1981) The bond-valence method: An empirical approach to chemical structure and bonding. In M. O'Keeffe and A. Navrotsky, Eds., Structure and bonding in crystals, vol. II, p. 1–30. Academic Press, New York.

Černá, Iva, Černý, Petr, and Ferguson, R.B. (1973) The fluorine content and some physical properties of the amblygonite-montebrasite minerals. American Mineralogist, 58, 291–301.

Dubois, J., Marchand, J., and Bourguignon, P. (1972) Données minéralogiques sur la série amblygonite-montebrasite. Annales de la Société Géologiques de Belgique, 95, 285–310.

Fleischer, Michael (1987) Glossary of mineral species (5th edition). The Mineralogical Record, Inc., Tucson.

Foord, E.E., Oakman, M.R., and Maxwell, C.H. (1985) Durangite from the Black Range, New Mexico, and new data on durangite from Durango and Cornwall. Canadian Mineralogist, 23, 241–246.

Fransolet, André-Mathieu. (1989) The problem of Na-Li substitution in primary Li-Al phosphates: New data on lacroixite, a relatively widespread mineral. Canadian Mineralogist, 27, 211–217.

Fransolet, André-Mathieu, and Tarte, Pierre. (1977) Infrared spectra of analyzed samples of the amblygonite-montebrasite series: A new rapid semi-quantitative determination of fluorine. American Mineralogist, 62, 559–564.

Fyfe, C.A., Gobbi, G.C., Hartman, J.S., Lenkinski, R.E., O'Brien, J.S., Beange, E.R., and Smith, M.A.R. (1982) High resolution solid state MAS spectra of ^{29}Si, ^{27}Al, ^{11}B and other nuclei in inorganic systems using a narrow bore 400 MHz high resolution NMR spectrometer. Journal of Magnetic Resonance, 47, 168–178.

Greiner, D.J. (1986) Influence of fluorine versus hydroxyl content on the optics of the amblygonite-montebrasite series. M.S. thesis, Virginia Polytechnic Institute and State University, Blacksburg, Virginia, 41 p.

Greiner, D.J., and Bloss, F.D. (1987) Amblygonite-montebrasite optics: Response to (OH^-) orientation and rapid estimation of F from $2V$. American Mineralogist, 72, 617–624.

Groat, L.A., Hawthorne, F.C., Carter, R.T., and Ercit, T.S. (1985) Tantalian niobian titanite from the Irgon Claim, Southeast Manitoba. Canadian Mineralogist, 23, 569–571.

Groat, L.A., Raudsepp, M., Hawthorne, F.C., Sherriff, B.L., and Hartman, J.S. (1987a) OH = F substitution across the amblygonite-montebrasite series: Crystal structure, infrared and MAS NMR spectroscopy. Geological Association of Canada/Mineralogical Association of Canada Program with Abstracts, 12, 49.

——— (1987b) OH = F substitution in the amblygonite-montebrasite series: A crystal structure and spectroscopic study. (Abs.) International Union of Crystallography, XIVth Congress and General Assembly, Perth, Australia.

Hawthorne, F.C., and Groat, L.A. (1985) The crystal structure of wroewolfeite, a mineral with $[Cu_4(OH)_6(SO_4)(H_2O)]$ sheets. American Mineralogist, 70, 1050–1055.

Hawthorne, F.C., Groat, L.A., Raudsepp, Mati, and Ercit, T.S. (1987) Kieserite, $Mg(SO_4)(H_2O)$, a titanite-group mineral. Neues Jahrbuch für Mineralogie Abhandlungen, 157, 121–132.

Herzfeld, J., and Berger, A.E. (1980) Sideband intensities in NMR spectra of samples spinning at the magic angle. Journal of Chemical Physics, 73, 6021–6030.

Higgins, J.B., and Ribbe, P.H. (1976) The crystal chemistry and space groups of natural and synthetic titanites. American Mineralogist, 61, 878–888.

——— (1977) The structure of malayaite, $CaSnOSiO_4$, a tin analogue of titanite. American Mineralogist, 62, 801–806.

International Tables for X-ray Crystallography, (1974) vol. IV. Kynoch Press, Birmingham, England.

Isaacs, A.M., and Peacor, D.R. (1981) Panasqueirite, a new mineral: The OH-equivalent of isokite. Canadian Mineralogist, 19, 389–392.

Kallio, Pekka. (1978) A new X-ray method for the estimation of fluorine content in montebrasites. American Mineralogist, 63, 1249–1251.

Maricq, M.M., and Waugh, J.S. (1980) NMR in a rotating solid. Journal of Chemical Physics, 70, 3300–3316.

Mongiorgi, R., and Riva di Sanseverino, L. (1968) A reconsideration of the structure of titanite, $CaTiOSiO_4$. Mineralogica et Petrographica Acta, 14, 123–141.

Moore, P.B. (1970) Structural hierarchies among minerals containing octahedrally coordinating oxygen: I. Stereoisomerism among corner-sharing octahedral and tetrahedral chains. Neues Jahrbuch für Mineralogie Monatshefte, 1970, 163–173.

Moss, A.A., Fejer, E.E., and Embrey, P.G. (1969) On the X-ray identification of amblygonite and montebrasite. Mineralogical Magazine, 37, 414–422.

Pajunen, Aarne, and Lahti, S.I. (1985) New data on lacroixite, $NaAlFPO_4$. Part II. Crystal structure. American Mineralogist, 70, 852–855.

Parise, J.B., Cuff, Cristopher, and Moore, F.H. (1980) A neutron diffraction study of topaz: Evidence for a lower symmetry. Mineralogical Magazine, 43, 943–944.

Paul, B.J., Černý, Petr, Chapman, Ron, and Hinthorne, J.R. (1981) Niobian tantalite from the Huron Claim pegmatite, southeasern Manitoba. Canadian Mineralogist, 19, 549–552.

Phillips, W.R., and Griffen, D.T. (1981) Optical mineralogy: The nonopaque minerals, p. 77–79. W. H. Freeman and Co., San Francisco.

Pistorius, C.W.F.T. (1960) Lattice constants of $FeSO_4 \cdot H_2O$ (artificial szomolnokite) and $NiSO_4 \cdot H_2O$. Bulletin Société del Belgique, 69, 570–574.

——— (1961a) Crystallographic properties of $CuSO_4 \cdot H_2O$ and $ZnSO_4 \cdot H_2O$. Acta Crystallographica, 14, 534.

——— (1961b) Crystallographic data for manganese (II) sulphate monohydrate (artificial szmikite). Zeitschrift für Anorganische und Allgemeine Chemie, 307, 226–228.

Raudsepp, M., Turnock, A.C., Hawthorne, F.C., Sherriff, B.L., and Hartman, J.S. (1987) Characterization of synthetic pargasitic amphiboles $(NaCa_2Mg_4M^{3+}Si_6Al_2O_{22}(OH,F)_2$; M^{3+} = Al, Cr^{3+},Ga,Fe^{3+},Sc,In) by infrared spectroscopy, Rietveld structure refinement, and ^{27}Al and ^{29}Si MAS NMR spectroscopy. American Mineralogist, 72, 580–593.

Rothwell, W.P., Waugh, J.S., and Yesinowksi, J.P. (1980) High resolution variable temperature ^{31}P NMR of solid calcium phosphates. Journal of the American Chemical Society, 102, 2637–2643.

Shannon, R.D. (1976) Revised effective ionic radii and systematic studies of interatomic distances in halides and chalcogenides. Acta Crystallographica, A32, 751–767.

Sheldrick, G.M. (1981) Nicolet SHELXTL Operations Manual. Nicolet XRD Corp., Madison, Wisconsin.

Simonov, W.I., and Belov, N.W. (1958) Die Aufklärung der Struktur des Amblygonits mit Hilfe der Minimumfunktion. Kristallografia 3, 428–437.

Taylor, M., and Brown, G.E. (1976) High-temperature structural study of the $P2_1/a = A2/a$ phase transition in synthetic titanite, $CaTiSiO_5$. American Mineralogist, 61, 435–447.

Yesinowski, J.P., and Mobley, M.J. (1983) ^{19}F MAS NMR of fluoridated hydroxyapatite surfaces. Journal of the American Chemical Society, 105, 6191–6193.

Manuscript received October 23, 1989
Manuscript accepted August 10, 1990